

# Resolving IRAS 09111 – 1007 at 350 microns: a different path to ULIRG formation?

Sophia A. Khan<sup>1,2</sup>, Dominic J. Benford<sup>2</sup>, David L. Clements<sup>1</sup>, S. Harvey Moseley<sup>2</sup>, Richard A. Shafer<sup>2</sup>, Timothy J. Sumner<sup>1</sup>

<sup>1</sup>*Imperial College London, Blackett Laboratory, Prince Consort Road, London SW7 2AZ, UK*

<sup>2</sup>*Infrared Astrophysics Branch, Code 685, NASA/GSFC, Greenbelt, MD 20771, USA*

25 January 2019

## ABSTRACT

We have resolved the ultraluminous infrared galaxy (ULIRG), IRAS 09111 – 1007, with the new 350  $\mu\text{m}$ -optimised Second Generation Submillimeter High Angular Resolution Camera (SHARC II) and present the first submillimetre fluxes and images for the system. IRAS 09111 – 1007 comprises two interacting luminous infrared galaxies (LIRGs) with a projected nuclear separation of  $39\text{ h}_{71}^{-1}\text{ kpc}$ . The Western galaxy is roughly four times more luminous in the submillimetre than its Eastern counterpart. It is an extremely bright LIRG with an AGN. The classification of the Eastern source is uncertain: it could be a Seyfert 2 galaxy or a LINER. We highlight IRAS 09111 – 1007 as a system that necessitates further study: a double AGN ULIRG whose molecular gas content differs from other widely separated pairs and whose ULIRG phase might not be explained by current multiple merger and/or final stage ULIRG scenarios.

**Key words:** infrared: galaxies – galaxies: starburst – galaxies: Seyfert – galaxies: interactions – galaxies: individual: IRAS 09111 – 1007

## 1 INTRODUCTION

Amongst the first results of extragalactic mid-IR astronomy was the discovery of a small number of galaxies that emit the bulk of their bolometric luminosity in the infrared (Low & Kleinmann 1968, Kleinmann & Low 1970a,b). The InfraRed Astronomical Satellite, IRAS, detected large numbers of these ultraluminous infrared galaxies (ULIRGs) (Soifer et al. 1984, Joseph & Wright 1985, and Soifer, Neugebauer & Houck 1987) with quasar-like luminosities of  $L_{\text{IR}}(8\text{--}1000\text{ }\mu\text{m}) > 10^{12} L_{\odot}$ . There is still debate as to the nature of the far-IR power source in these galaxies: is the immense thermal energy driven by a dominant starburst, a dominant AGN or some combination of the two? These low-redshift IRAS-selected ULIRGs are expected to be the counterparts to the high redshift ( $z > 1$ ) SCUBA sources (see, e.g., Smail et al. 1998, Blain et al. 2002, Webb et al. 2003, Chapman et al. 2003).

Most ULIRG systems have been shown to be disturbed, interacting or merging in some way when the separation of nuclei is less than 10kpc (Sanders et al. 1988, Clements et al. 1996, Murphy et al. 1996, Farrah et al. 2001). The nature of widely separated ULIRG systems is less clear (Dinh-V-Trung et al. 2001, Meusinger et al. 2001): are the components of the ULIRG (supposedly the end phase of the galactic interaction) beginning another merger or is the

ULIRG a result of a multiple merger event (Borne et al. 2000)? This latter scenario is possible in widely separated ULIRGs with resolved double nuclei but might not apply to the ULIRG system IRAS 09111 – 1007, which consists of two widely spaced but interacting luminous infrared galaxies (LIRGs), each with a single nucleus. The two LIRGs have a projected separation of  $39\text{ h}_{71}^{-1}\text{ kpc}$  and a velocity difference of  $425\text{ km s}^{-1}$  (Duc, Mirabel & Maza 1997). In this letter we present 350  $\mu\text{m}$  resolved images and fluxes for IRAS 09111 – 1007. We model the far-IR dust emission to constrain the nature of the interaction.

## 2 OBSERVATIONS AND DATA REDUCTION

The data were taken using the Second Generation Submillimeter High Angular Resolution Camera (SHARC II) at the Caltech Submillimeter Observatory on Mauna Kea, Hawai'i, in January and March 2004. SHARC II is a 350  $\mu\text{m}$ -optimised camera (Dowell et al. 2003) built around a  $12 \times 32$  element close-packed bolometer array (Moseley et al. 2004). It achieves a point-source sensitivity of  $\sim 1\text{ Jy Hz}^{-1/2}$  in good weather. The 384 pixels of the SHARC II array image a region of around  $1.0' \times 2.5'$ . Its filled absorber array provides instantaneous imaging of the entire field of view, sampled at roughly 2.5 pixels per nominal beam area. The

| Name               | Coordinates<br>(J2000) | 350 $\mu$ m Flux<br>[Jy] | log(L <sub>FIR:SED</sub> )<br>[L <sub>⊙</sub> ] | log(L <sub>FIR:IRAS</sub> )<br>[L <sub>⊙</sub> ] | log(L <sub>IR</sub> )<br>[L <sub>⊙</sub> ] | SFR<br>[M <sub>⊙</sub> yr <sup>-1</sup> ] |
|--------------------|------------------------|--------------------------|---|--|--|---|
| IRAS 09111 – 1007  |                        |                          | 11.91   | 11.86  | 12.09                                      | 81  |
| IRAS 09111 – 1007W | 09 13 36.4 -10 19 31.8 | 0.85±0.13                | 11.80   | 11.75  | 11.98                                      | 63  |
| IRAS 09111 – 1007E | 09 13 38.8 -10 19 21.5 | 0.23±0.04                | 11.25   | 11.20  | 11.43                                      | 18  |

**Table 1.** Coordinates, 350 $\mu$ m fluxes, luminosities and star formation rates for the system and both components of IRAS 09111 – 1007 (IRAS fluxes from Surace, Sanders & Mazzarella 2004). The FIR (40 – 500  $\mu$ m) and IR (8 – 1000  $\mu$ m) luminosities are derived as follows: L<sub>FIR:SED</sub> is computed from best-fitting single temperature SED, L<sub>FIR:IRAS</sub> and L<sub>IR</sub> are calculated using the standard relations from Fullmer & Lonsdale (1989) and Sanders & Mirabel (1996) respectively. Note that the pair positions given in both NED and Surace, Sanders & Mazzarella (2004) are swapped.

beam profile was measured on known compact sources, and was verified to be within five per cent of the diffraction-limited beamwidth of 8.5''.

For these data the in-band zenith atmospheric opacity ( $\tau_{350\mu\text{m}}$ ) ranged from 1.1 to 1.3, corresponding to a zenith transmission of around 30 per cent. Our observations were centred on the Eastern source of the pair, at position RA=09<sup>h</sup>13<sup>m</sup>38.<sup>s</sup>6, Dec=−10°19′20'' (J2000).

In the submillimetre, emission from the atmosphere dominates the signal read out by the bolometers. In order to detect the faint celestial sources it is necessary to remove this emission. The sky signal, however, is largely correlated between pixels. At any moment in time, every pair of pixels can be used as a ‘signal’ beam and a ‘reference’ beam. Additionally, the telescope is moved such that each position on the sky can be viewed by many detectors at different times. This introduces a self-consistent self-calibration of all pixels compared with all others. A Lissajous scan pattern is used to ensure that the area on the sky is well covered and has substantial redundancy of observing.

The data were reduced using the standard CSO reduction software, CRUSH (Kovács, in preparation). This software implements a self-consistent least-squares algorithm to solve for the celestial emission, taking into account instrumental and atmospheric contributions to the signal. All observations were taken using the Dish Surface Optimisation System (Leong 2003), which corrects for the primary mirror deformation as a function of zenith angle, to improve the telescope efficiency and the pointing.

The skymap is calibrated with a point spread function based on all point source observations (Callisto, Ceres & Arp 220) through the observing period at similar elevations. An oversampled  $\chi^2$  fit is used to determine the position of the source and the flux per beam. The processed image is shown in Figure 1.

### 3 RESULTS

We are able to resolve the IRAS 09111 – 1007 system and obtain 350  $\mu$ m fluxes and positions. An absolute pointing offset of 2.0'' ( $\Delta\alpha = 1.0''$ ,  $\Delta\delta = 1.7''$ ) from the 2MASS positions was attributed to a pointing error (due to the imprecise absolute pointing knowledge of the CSO) and removed from the SHARC II image presented in this letter.

The brighter LIRG, that which contributes  $\approx 79$  per cent of the total system 350  $\mu$ m emission, is known as the ‘Western source’ or IRAS 09111 – 1007W for the purposes of this

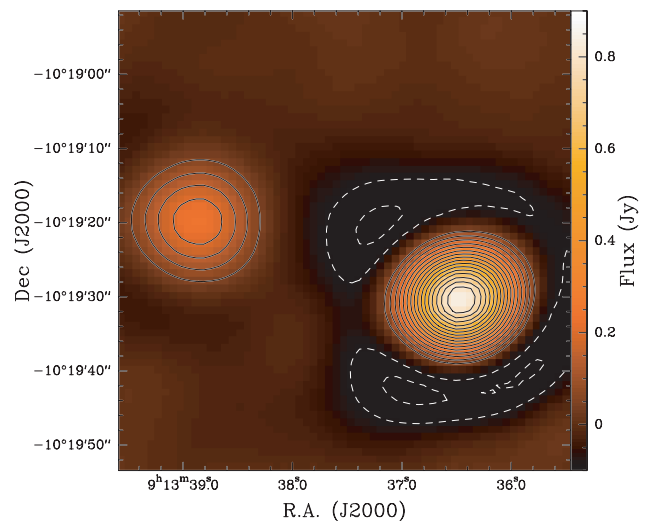


**Figure 1.** 350  $\mu$ m continuum emission map of IRAS 09111 – 1007 taken with SHARC II. The contours are in levels of 50 mJy/beam (dashed contours are negative and are an artifact of data reduction).

letter. The Eastern LIRG is called the ‘Eastern source’ or IRAS 09111 – 1007E (Murphy et al. 1996). Together they form the ‘ULIRG system’. Figure 2 shows the resolved components of IRAS 09111 – 1007 imaged with the DSS, 2MASS and IRAS (HIRES processed; Surace, Sanders & Mazzarella 2004) respectively. The 350  $\mu$ m fluxes for each component are presented in Table 1. The signal-to-noise in the detection is 89 for the Western source and 29 for the Eastern source. The Western source is roughly four times more luminous in the submillimetre than its Eastern counterpart.

### 4 SED MODELLING

#### 4.1 Dust Temperature Blackbody Fitting

A modified blackbody is used to model the total dust emission of the IRAS 09111 – 1007 system, specifically:

$$F_\nu = (M_{\text{dust}}/D^2)\kappa(\lambda)B_\nu(\lambda, T_{\text{dust}}) \quad (1)$$

where  $B_\nu$  is the Planck function,  $\kappa$  the mass absorption coefficient of the dust ( $\kappa(\lambda) \propto \lambda^{-\beta}$ , see Dwek 2004),  $T_{\text{dust}}$  and  $M_{\text{dust}}$  the equilibrium dust temperature and mass respectively, and  $D$  the distance of the galaxy. For the distance we

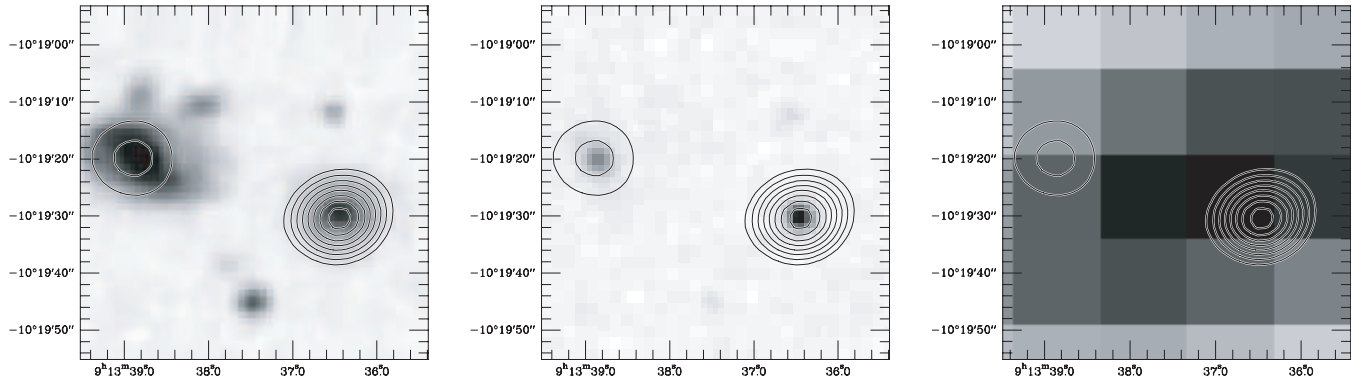


**Figure 2.** DSS Optical, 2MASS  $K_s$ , and IRAS  $60\,\mu\text{m}$  images of IRAS 09111 – 1007, with  $350\,\mu\text{m}$  contours overlaid on each (in levels of 100 mJy/beam).

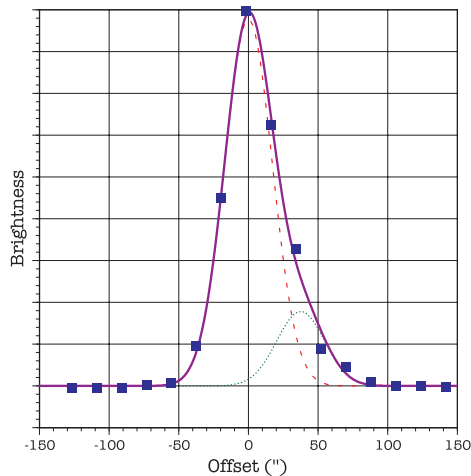


**Figure 3.** Fit to the spatial variation in intensity for the HIRES-processed IRAS  $60\,\mu\text{m}$  image, cut through both galaxies.

use WMAP cosmology ( $H_0 = 71\,\text{km s}^{-1}\,\text{Mpc}^{-1}$ ,  $\Omega_m = 0.27$ , and  $\Omega_\Lambda = 0.73$  (Bennett et al. 2003)).

In order to better constrain the SED of each component, we determined the ratio of the fluxes of the two components at  $60\,\mu\text{m}$ . Beginning with the IRAS  $60\,\mu\text{m}$  HIRES-processed image of Surace et al. (2004), we sliced along the axis of the known  $350\,\mu\text{m}$  sources. A pair of Gaussian intensity functions were fitted to the measured flux along this slice, constraining them to have the same width and a fixed spacing as determined at  $350\,\mu\text{m}$  (see Figure 3). The remaining four free parameters (one position, the width, and the two intensities) are then well-constrained, with the flux ratio being  $4.9 \pm 0.8$  (the total system flux as measured by IRAS is still valid, since the IRAS fluxes are derived with an aperture large compared to the source separation). The ratio derived from the  $350\,\mu\text{m}$  measurement is  $3.7 \pm 1.1$ . Alternatively, the fraction of the flux from the brighter LIRG is  $83 \pm 3$  per cent at  $60\,\mu\text{m}$  and  $79 \pm 16$  per cent at  $350\,\mu\text{m}$ , an entirely consistent measurement. The ratio of 79 per cent is accurate enough for the fits that follow.

$\chi^2$  minimization determined the best-fitting emissivity index ( $\beta$ ) and corresponding single fit dust temperature for the system using the SHARC II  $350\,\mu\text{m}$  flux with the  $60\,\mu\text{m}$

| Model  | Source         | $\beta$        | $T_{\text{dust}}$<br>[K] | $M_{\text{dust}}$<br>[ $10^6 M_\odot$ ] |
|--|----------------|----------------|--------------------------|---|
| Single Temperature                                     | System         | $1.9 \pm 0.1$  | $31 \pm 1$               | $220^{+30}_{-20}$                       |
|  | Western source | $1.9 \pm 0.1$  | $31 \pm 1$               | $170^{+30}_{-20}$                       |
|  | Eastern source | $1.9 \pm 0.1$  | $31 \pm 1$               | $50^{+10}_{-10}$                        |
| Two Temperature<br>$M_{\text{cold}}/M_{\text{warm}}=1$ | System         | 2.0<br>(fixed) | $32 \pm 2$<br>$26 \pm 5$ | $300^{+190}_{-110}$                     |
|  | System         | 2.0<br>(fixed) | $36 \pm 3$<br>$29 \pm 1$ | $280^{+70}_{-50}$                       |
| Single Temperature<br>DL Dust Model                    | System         | n/a            | $30 \pm 1$               | $250^{+30}_{-30}$                       |
|  | Western source | n/a            | $30 \pm 1$               | $200^{+30}_{-30}$                       |
|  | Eastern source | n/a            | $30 \pm 1$               | $60^{+10}_{-10}$                        |

**Table 2.** Best-fitting SED parameters:  $\beta$ , temperature and dust mass for the IRAS 09111 – 1007 system and components, with corresponding estimated  $1\sigma$  uncertainties.

and  $100\,\mu\text{m}$  IRAS fluxes derived in Surace et al. (2004) (the  $100\,\mu\text{m}$  flux was used as the normalization). The best-fitting was  $\beta=1.9\pm0.1$ ,  $T=31\pm1\,\text{K}$ , and is shown in Figure 4. We also model both the Western and Eastern sources assuming that the IRAS fluxes are distributed in the same way as the  $350\,\mu\text{m}$  emission. Dust masses are calculated assuming the  $100\,\mu\text{m}$  mass absorption coefficient,  $\kappa_{100}$ , is  $40\,\text{cm}^2\,\text{g}^{-1}$  (Draine & Lee 1984).

With only two independent colours we cannot constrain the cold and warm dust masses and simultaneously fit the dust temperatures in a two temperature model. Using  $\beta=2$  (as in Dunne & Eales 2001), if we assume equal amounts of cold and warm dust in the system we get best-fitting temperatures of  $T_{\text{cold}} = 26 \pm 5\,\text{K}$  and  $T_{\text{warm}} = 32 \pm 2\,\text{K}$ . If we adopt a dust mass distribution typical of the highest luminosity galaxies from the SCUBA Local Universe Galaxy Survey (SLUGS), as given in Dunne & Eales (2001), we get a ratio  $M_{\text{cold}}/M_{\text{warm}}=11$ . The best-fitting values are then  $T_{\text{cold}} = 29 \pm 1\,\text{K}$ ,  $T_{\text{warm}} = 36 \pm 3\,\text{K}$ .

As an alternative to these approaches, we also used a more physically-based dust grain model (the single temperature DL dust model – Draine & Lee 1984, Laor & Draine 1993), an equal mixture of silicates and graphites with  $\kappa_{100}$  of 31 and  $54\,\text{cm}^2\,\text{g}^{-1}$  for the silicate and graphite grains re-

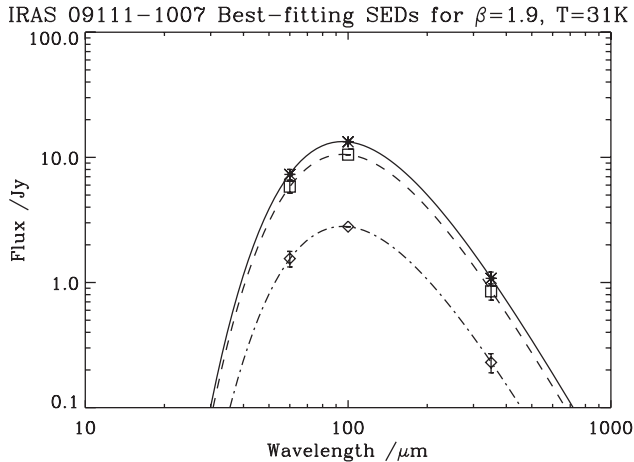


**Figure 4.** Single Temperature Best-Fitting SED for the Western source (dashed), Eastern source (dot-dashed), and the IRAS 09111 – 1007 system (solid:  $\beta=1.9$ ,  $T=31$  K).

spectively. In this case, the best-fitting temperature of the system was  $30 \pm 1$  K.

The dust temperature of  $\sim 31$  K is within  $1.5\sigma$  of the average temperature of  $38 \pm 6$  K from the previous  $350 \mu\text{m}$  LIRG study by Benford (1999), with the first SHARC camera (although that survey did not include any widely separated LIRG systems). The result that the  $60 \mu\text{m}$  dust is distributed in very similar ratios to the  $350 \mu\text{m}$  dust (Figure 3) is responsible for the identical SED temperatures for both components.

## 4.2 Ratio of Molecular Gas To Dust

The molecular gas mass in the Western source is  $2.3 \times 10^{10} M_{\odot}$  (Mirabel et al. 1990). The Western source’s dust mass is derived from the best-fitting SED to give a molecular gas-to-dust ratio of 140 and 120 for the single temperature and DL dust models respectively. In the absence of 21 cm HI observations this value is a lower limit on the total (molecular + atomic) gas-to-dust ratio.

The 8–1000  $\mu\text{m}$  luminosity ( $L_{\text{IR}}$ , see Table 1) gives a value for the Western source IR luminosity-to- $\text{H}_2$  mass ratio ( $L_{\text{IR}}/M(\text{H}_2)$  – the star formation efficiency) of  $42 L_{\odot} M_{\odot}^{-1}$ . The molecular gas-to-dust and IR luminosity-to- $\text{H}_2$  mass ratios are consistent with values for the highest luminosity SLUGS galaxies (Dunne et al. 2000).

Dinh-V-Trung et al. (2001) studied six widely separated ( $> 20$  kpc) ULIRG systems in the complete 1 Jy sample of Kim & Sanders (1998). In their sample, the molecular gas was concentrated in the dominant source of the far-IR emission. Although the Western source of IRAS 09111 – 1007 is gas-rich, the Eastern source, by virtue of the amount of dust, is unlikely to be gas-poor. This would make this system different from their wide-pair ULIRG sample.

## 4.3 Star Formation Rate

The system and component luminosities (see Table 1) show that the two components form a ULIRG system, though neither is a ULIRG individually. The star formation rate

in Table 1 uses the SED derived FIR luminosities and the relation of Thronson & Telesco (1986):

$$\text{SFR} \sim \Psi 10^{-10} \left( \frac{L_{\text{FIR}}}{L_{\odot}} \right) M_{\odot} \text{ yr}^{-1} \quad (2)$$

assuming  $\Psi = 1$  (typical values of  $\Psi$  are 0.8–2.1).

## 5 DISCUSSION

### 5.1 Source Characterisation

The optical image from the Digitized Sky Survey (Figure 2, left) shows the disturbed morphology of the Eastern source. In the 2MASS  $K_s$  band image (Figure 2, centre) the Western source is slightly more luminous than the Eastern, a trait even more prominent in the submillimetre (Figure 1). Merger models such as Barnes & Hernquist (1991) predict gas and dust to be concentrated in the galaxy centre as the ULIRG interaction condenses large amounts of the ISM into the nuclear region.

Line ratios from Duc et al. (1997) classify the Western source as a Seyfert 2. Dudley (1999) found prominent polycyclic aromatic hydrocarbon features in the 8–13  $\mu\text{m}$  dust emission spectra – indicative of a starburst. The Eastern source is either a Seyfert 2 or LINER galaxy (Duc et al. 1997), while Gonçalves, Véron-Cetty & Véron (1999) also find evidence for a starburst. Neither of the two sources in the IRAS 09111 – 1007 system were detected in the ROSAT All-Sky Survey. A non-detection in the ROSAT band does not necessarily mean that a source is intrinsically weak since the soft X-ray band is sensitive to X-ray absorption, which is common in AGN.

### 5.2 Merging Stage

Without additional submillimetre data we are unable to constrain the relative temperatures and masses of the cold and warm dust components. Whether the dust temperature of the system is related to the stage of merging is not clear. Mazzarella, Bothun & Boroson (1991) find an increase in warm dust temperature with merging stage, although Klaas et al. (2001) argue the cold dust temperature would increase as well. The wide separation of the pair would suggest that IRAS 09111 – 1007 is at the beginning of a merger, a notion supported by the value of the IR luminosity-to- $\text{H}_2$  mass ratio, which falls within a region of  $L_{\text{IR}}/M(\text{H}_2)$  vs  $L_{\text{IR}}$  space that is common for early merging systems (Sanders, Scoville & Soifer 1991).

### 5.3 Widely Spaced ULIRG Pairs

Unlike the wide pair sample of Xu & Sulentic (1991) *both* components are enhanced in the far-IR. With a velocity difference of  $425 \text{ km s}^{-1}$  (Duc et al. 1997) and a projected separation of  $39 h_{71}^{-1} \text{ kpc}$ , Monte Carlo simulations give the probability of the pair being bound as 0.88 (Schweizer 1987).

Although widely separated ULIRG pairs are not uncommon the nature of their interaction is still uncertain. Murphy et al. (1996) postulated the presence of a third nucleus in widely separated pairs, though no double nucleus has been detected in either component of IRAS 09111 – 1007. The

galaxies were shown to be unresolved at  $0.''5$  resolution in a 6 cm search by Crawford et al. (1996). However the non-detection of a double nucleus cannot rule out a multiple merger since the time-scale of nuclei coalescence is short (Surace, Sanders & Evans 2000, Meusinger et al. 2001). In multiple approach merger models (e.g., Dubinski, Mihos & Hernquist 1999) the merging process is a series of encounters where bound components approach and separate. A previous encounter may have triggered the starburst/AGN in the system. High resolution optical imaging (Borne et al. 2000) could decide between these scenarios by either detecting multiple nuclei or confirming single nuclei. High resolution CO imaging would be needed to detect whether gas has been disturbed by a previous phase of the merging event (Mihos & Hernquist 1996).

## 6 CONCLUSIONS

We have resolved the widely separated ULIRG system of IRAS 09111 – 1007 with the SHARC II detector at  $350\ \mu\text{m}$ . This system comprises two LIRGs with a projected separation of  $39\ h_{71}^{-1}\ \text{kpc}$ , or around two optical diameters. The Western component dominates the far-IR flux at both  $60\ \mu\text{m}$  and  $350\ \mu\text{m}$ , carrying 79 per cent of the total system luminosity. Although the luminosity of the system is large, our fluxes suggest a dust temperature of 31 K for this system, with both components at the same temperature to within the sensitivity of this measurement. The wide separation and the value of the IR luminosity-to- $\text{H}_2$  mass ratio suggest that the pair are at an early stage of interaction. But the high luminosity of the system ( $L_{\text{IR}} = 1.2 \times 10^{12}\ L_{\odot}$ ) would be unusual for such a stage, unless the components had experienced a previous merger or interaction. A high resolution optical search for multiple nuclei within each component is needed. Their absence could indicate that the double AGN-LIRG system of IRAS 09111 – 1007, and perhaps other widely spaced ULIRG pairs, might be unexplained by current theories of ULIRG formation and evolution.

## 7 ACKNOWLEDGMENTS

This research has made use of the NASA/IPAC Extragalactic Data base (NED), which is operated by the Jet Propulsion Laboratory under contract with NASA. The optical image is taken from photographic data obtained using the UK Schmidt Telescope. The Caltech Submillimeter Observatory is supported by NSF contract AST-0229008.

We thank the anonymous referee for their insightful and careful comments. We are very grateful to Pierre-Alain Duc for providing clarification and additional spectroscopic data for the system, to Jason Surace for providing his HIRES-processed IRAS images, to Eli Dwek for SED discussion and the DL dust model, and to Rick Arendt for invaluable IDL data analysis advice. We extend our thanks to Tom Phillips and the CSO for our observing time and support during our runs, Hiroshige Yoshida for undertaking heterodyne observations on our behalf, and to Darren Dowell, Attila Kovács, and Colin Borys for observation and instrument assistance and support with data analysis.

## 8 REFERENCES

- Barnes J.E., Hernquist L.E., 1991, *ApJ*, 370L, 65  
 Benford D.J., 1999, PhD thesis, Caltech  
 Bennett C.L., et al., 2003, *ApJS*, 148, 1  
 Blain A.W., Smail I., Ivison R.J., Kneib J.-P., Frayer D.T., 2002, *PhR*, 369, 111  
 Borne K.D., et al., 2000, *ApJ*, 529L, 77  
 Chapman S.C., Blain A.W., Ivison R.J., Smail I.R., 2003, *Nature*, 422, 695  
 Clements D.L., Sutherland W.J., McMahon R.G., Saunders W., 1996, *MNRAS*, 279, 477  
 Crawford, T., Marr, J., Partridge, B., Strauss, M.A., 1996, *ApJ*, 460, 225  
 Dinh-V-Trung, Lo K.Y., Kim D.-C., Gao Y., Gruendl R.A., 2001, *ApJ*, 556, 141  
 Dowell C.D., et al., 2003, *SPIE*, 4855, 73  
 Draine B.T., Lee H.M., 1984, *ApJ*, 285, 89  
 Dubinski J., Mihos J.C., Hernquist L., 1999, *ApJ*, 526, 607  
 Duc P.-A., Mirabel I.F., Maza J., 1997, *A&AS*, 124, 533  
 Dudley C.C., 1999, *MNRAS*, 307, 553  
 Dunne L., Eales S., Edmunds M., Ivison R., Alexander P., Clements D.L., 2000, *MNRAS*, 315, 115  
 Dunne L., Eales S.A., 2001, *MNRAS*, 327, 697  
 Dwek E., 2004, *ApJ*, 607, 848  
 Farrah D., et al., 2001, *MNRAS*, 326, 1333  
 Fullmer L., Lonsdale C.J., 1989, *JPL D-1932*, Version 2, part no 3  
 Gonçalves A.C., Véron-Cetty M.P., Véron P., 1999, *A&AS*, 135, 437  
 Joseph R.D., Wright G.S., 1985, *MNRAS*, 214, 87  
 Kim D.-C., Sanders D.B., *ApJS*, 1998, 119, 41  
 Klaas U., et al., 2001, *A&A*, 379, 823  
 Kleinmann D.E., Low F.J., 1970a, *ApJ*, 159L, 165  
 Kleinmann D.E., Low, F.J., 1970b, *ApJ*, 161L, 203  
 Laor A., Draine B.T., 1993, *ApJ*, 402, 441  
 Leong M., 2003, <http://www.cso.caltech.edu/dsos/DSOSAMOSpaper.htm>  
 Low J., Kleinmann D.E., 1968, *AJ*, 73, 868  
 Mazzarella J.M., Bothun G.D., Boroson T.A., 1991, *ApJ*, 101, 2034  
 Meusinger H., Stecklum B., Theis C., Brunsendorf J., 2001, *A&A*, 379, 845  
 Mihos J.C., Hernquist L., 1996, *ApJ*, 464, 641  
 Mirabel I.F., Booth R.S., Johansson L.E.B., Garay G., Sanders D.B., 1990, *A&A*, 236, 327  
 Moseley S.H., Allen C.A., Benford D., Dowell C.D., Harper D.A., Phillips T.G., Silverberg R.F., Staguhn J., 2004, *NIMPA*, 520, 417  
 Murphy T.W., Jr, Armus L., Matthews K., Soifer B.T., Mazzarella J.M., Shupe D.L., Strauss M.A., Neugebauer G., 1996, *AJ*, 111, 1025  
 Sanders D.B., Soifer B.T., Elias J.H., Madore B.F., Matthews K., Neugebauer G., Scoville N.Z., 1988, *ApJ*, 325, 74  
 Sanders D.B., Scoville N.Z., Soifer B.T., 1991, *ApJ*, 370, 158  
 Sanders D.B., Mirabel I.F., 1996, *ARA&A*, 34, 749  
 Schweizer L.Y., 1987, *ApJS*, 64, 427  
 Smail I., Ivison R.J., Blain A.W., Kneib J.-P., 1998, *ApJ*, 507L, 21  
 Soifer B.T., et al., 1984, *ApJ*, 278L, 71  
 Soifer B.T., Neugebauer G., Houck J.R., 1987, *ARA&A*,

25, 187

Surace J.A., Sanders D.B., Evans A.S., 2000, ApJ, 529, 170

Surace J.A., Sanders D.B., Mazzarella J.M., 2004, AJ, 127, 3235

Thronson H., Telesco C., 1986, ApJ, 311, 98

Webb T.M.A, Lilly S.J., Clements D.L., Eales S., Yun M.,

Brodwin M., Dunne L., Gear W.K., 2003, ApJ, 597, 680

Xu C., Sulentic J.W., 1991, ApJ, 374, 407